Imaging the Reaction Dynamics of OH + CD_4. 2. Translational Energy Dependencies

Bailin Zhang,† Weicheng Shiu,† and Kopin Liu*,†,‡

Institute of Atomic and Molecular Sciences (IAMS), Academia Sinica, P.O. Box 23−166, Taipei, Taiwan 10617, and Department of Chemistry, National Taiwan University, Taipei, Taiwan 10617

Received: July 5, 2005; In Final Form: August 7, 2005

The reaction of OH + CD_4 is investigated in a crossed-beam experiment over the collisional energies ranging from reaction threshold of about 5 to 16 kcal/mol. Exploiting a time-sliced ion velocity imaging detection scheme, the coincident information on the two polyatomic product pairs, HOD and CD_3, is revealed in a state-correlated manner. The recently discovered vibrational mode-correlation between the two products is found to persist over the full range of collision energies of this study. In addition, the energy dependencies of the correlated cross section, state distribution, and angular distribution are elucidated, providing an unprecedented insight into this important reaction.

I. Introduction

The hydrogen abstraction reaction from methane by a hydroxyl radical is of great importance in the combustion of fossil fuels.[1,2] The CH_3 radicals produced in this initiation step are subsequently oxidized to CO and CO_2 through a chain reaction mechanism. In addition, the OH + CH_4 reaction plays a significant role in atmospheric chemistry due to the relatively high abundance of CH_4 in the troposphere.[3] In fact, it constitutes one of the major processes for the removal of atmospheric methane, and is believed to be the primary process in regulating the steady-state concentration of OH radicals in the troposphere.[4] Therefore, the OH + CH_4 reaction has often been regarded as one of the key steps in building up models to help interpreting the atmospheric chemistry.[5] As a result of its practical importance, this reaction has received a great deal of attention in scientific communities. Experimentally, the rate constants have been measured using various techniques over a wide range of temperatures.[6,7] The reaction is exothermic by −14.31 kcal/mol, and has a rate coefficient of 8.3×10^{-15} cm^3 molecule s^{-1} at 298 K. Its temperature dependence exhibits a non-Arrhenius behavior; nonetheless, an approximate activation energy of 3.6 kcal/mol can be deduced.

Theoretically, this reaction has also been extensively studied using a variety of ab initio methods.[8−13] These investigations have been mainly concerned with the transition state structure and classical potential energy barrier height for calculating the thermal rate constants. The calculated barrier heights range around 6.1−7.9 kcal/mol, or 4.7−6.6 kcal/mol when the zero-point energy is included. These values are considerably higher than the experimental activation energy of ∼ 3.6 kcal/mol, suggesting that quantum mechanical tunneling through the barrier is important at low collision energies. The reported imaginary frequency at the saddle point varies from 1617 to 2075 cm^{-1}, indicating significant differences in the calculated shape of the potential energy surface (PES) near the transition state region. Despite the uncertainties, the computed rate constants using transition-state theory with tunneling correction are generally in good agreement with the experimental results.

There have been relatively few dynamical calculations for the OH + CH_4 reaction due to the lack of a suitable global PES. Using an empirical model potential and the rotating bond approximation, Nyman et al. investigated mode selectivity of this reaction,[14] as well as the effect on differential and integral cross sections by varying the potential energy in the entrance channel.[15] A five-dimensional quantum scattering model has also been developed and applied to this reaction.[16] The cumulative reaction probabilities from those studies indicated that the reaction occurs via a direct mechanism. Theories further predicted that vibrational excitations of CH_4 can enhance substantially the rate of reaction while exciting the OH stretch has negligible effect.[14,16] Thus, the reactant OH can be treated as a spectator in this reaction. For the ground-state OH + CH_4 reaction, the theoretical H_2O product vibration distributions are rather cold, but a considerable excitation in the umbrella mode of CH_3 product is predicted.[16]

The only experimental dynamics study of this reaction is the recent report from this laboratory on an isotopically analogous OH + CD_4 reaction (part 1 of this series).[17] A strong vibration mode-correlation of the product pairs, HOD and CD_3, was discovered. When the ground-state $CD_3(v = 0)$ is produced, over 90% of the coincidently formed HOD coproducts are *purely stretch-excited*, with an inverted distribution peaking at $v_{OD} = 2$ in the local mode representation. The observation of highly vibrational-excited HOD products is in striking contrast to the aforementioned theoretical prediction,[14] but it is in line with the results for an analogous OH + D_2 reaction.[18−20] By way of contrast, when CD_3 is produced with two-quantum excitation in the umbrella mode, a significant excitation of *stretch−bend combination* mode of HOD coproducts was observed. This was the first clear example of mode-correlation of product pairs from a chemical reaction.[17,21] The vibrationally state-specific angular distributions of $CD_3(v = 0)$ and $CD_3(v_2 = 2)$ products also exhibit significant difference. While a backward-peaking distribution was found for $CD_3(v = 0)$, a notable shift toward sideways was observed for $CD_3(v_2 = 2)$. In either case, only small variations among the individual pair-correlated differential cross section (CDCS) were noted. In ref 17, the experiment was performed under the condition that both $CD_3(v = 0)$ and $CD_3(v_2 = 2)$ were produced at approximately the same energies.

* Corresponding author. E-mail: kpliu@gate.sinica.edu.tw.
† Academia Sinica.
‡ National Taiwan University.

10.1021/jp0536605 CCC: $30.25
Published on Web 09/15/2005

In this report, (part 2), we extend the study to a wide energy range in order to investigate the translational energy dependencies of the mode-correlation behavior, and in the following paper (part 3), the dynamical consequence of the isotope effect will be elucidated.

II. Experiment

The crossed-beam scattering experiments were identical to that reported previously (part 1).[17] Only the key features are mentioned here. The reaction product CD_3 was detected state-selectively by the combination of a (2 + 1) resonance-enhanced multiphoton ionization (REMPI) scheme and a time-sliced, ion velocity imaging technique.[22] The correlated attributes of the coincidently formed HOD products were revealed directly from the velocity-mapped CD_3^+ ion images, by virtue of energy conservation. The ground state ($v = 0$) and the first overtone of umbrella-mode excited ($v_2 = 2$) CD_3 products were probed with 333 nm light through the 0_0° and 2_2° bands of the $\tilde{X}^2A'' \rightarrow\rightarrow 3p_z^2A''$ two-photon transition, respectively.[23] The cold OH radical beam was generated via a photolysis + reaction scheme as detailed previously.[17] To cover sufficiently wide range of collision energies, either a neat CD_4 or 20% CD_4 seeded in H_2 (for higher E_c) was used for the target beam. The beam speeds were determined from the time-of-flight measurements using two fast ionization gauges. The resulted uncertainty in E_c is typically ±0.2 kcal/mol. Depending on the signal strength, each image was acquired for 2−8 h at 20 Hz, accumulating to (4−16) × 10^4 events. The use of an Even−Lavie pulsed valve[24] increased the signal by ~ 3-fold compared to the piezoelectric valve,[22,23] which made this study possible. To ascertain the collisional energy dependency, independent experiments at many more E_c's were performed, for which the image of $CD_3(0_0^\circ)$ at each E_c was accumulated from 20 min to 1 h for a global view. Because of the low count rates, statistically only the information on CD_3 state-specific excitation function and the E_c dependence of total angular distribution, i.e., not the correlated state-pair attribute, can be reliably deduced from those measurements.

III. Results and Discussion

(A) Mode- and State-Correlation of Product Pairs. Figure 1 exemplifies two typical raw images of the state-selected $CD_3(v)$ product from the OH + CD_4 reaction. Both images, for $v = 0$ and $v_2 = 2$, are at the same collision energy of 16.2 kcal/mol. Superimposed on the image is the Newton diagram with the CD_3 product scattering angle indicated. The zero-degree means that the CD_3 product is scattered in the same direction as the incident CD_4 beam in the center-of-mass frame. While both images display several concentric ringlike features, their appearances are significantly different. In the case of $CD_3(v = 0)$, the angular distributions are broad and predominantly in the backward hemisphere, and the most intense ring feature is clearly the middle one. On the other hand, the angular distribution becomes mainly sideways for $CD_3(v_2 = 2)$, and the most prominent ring also changes. Hence, even just a casual inspection of the raw images reveals remarkable variations both in terms of the state-specific angular distribution and the correlated state distribution of the HOD coproducts.

In part 1 of this series,[17] the state-selected $CD_3(v)$ images were reported at somewhat lower collision energies, $E_c = 10.0$ kcal/mol for $v = 0$ and $E_c = 10.6$ and 13.6 kcal/mol for $v_2 = 2$. The two E_c's for $CD_3(v_2 = 2)$ were chosen at the time so that at 10.6 kcal/mol (or 13.6 kcal/mol) it has about the same initial energy (or available energy for disposal) as the ground-state $CD_3(v = 0)$ case. A strong mode correlation was discovered. When the ground-state $CD_3(v = 0)$ is produced, the coincidently formed HOD are mostly stretch-excited with two-quantum excitation in the newly born OD bond, which has 15.77 kcal/mol of vibrational energy.[25] When CD_3 is produced with two-quantum excitation in the umbrella mode, the most popular coproduct HOD state shifts to $v_{OD} = 1$ with 7.8 kcal/mol of vibrational energy,[25] and, perhaps more significantly, a substantial excitation in the stretch−bend combination mode is also induced. The question addressed in this work is as follows: How does the mode correlation vary with collision energies?

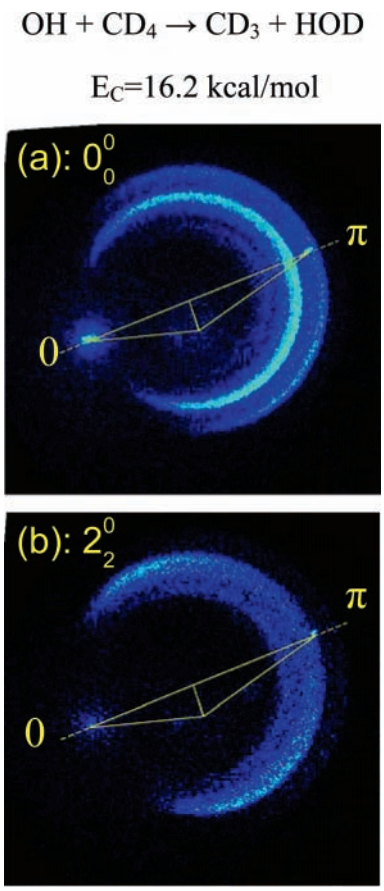

Figure 1. Two representative time-sliced raw images of the $CD_3(v = 0)$ and $CD_3(v_2 = 2)$ products from the title reaction at the collision energy of 16.2 kcal/mol. The probed REMPI bands are labeled and the Newton diagrams overlaid. The forward background appeared at the CD_4 beam velocity was experimentally verified and discarded in data analysis. Note the distinct ringlike structures of the two images.

Similar to previous studies, quantitative information on the images are obtained after the density-to-flux transformation.[22,26] Figure 2 illustrates a few CD_3-product speed distributions thus derived. The results for the two images in Figure 1 are presented on the left. The aforementioned intensity variations among the ring features of the two raw images are now quantitatively reflected in the different patterns of the $P(\mu)$ distributions. The energetics of the images are well-defined: $\Delta H_{rx} = -13.73$ kcal/mol, $E_c = 16.2$ kcal/mol. The CD_3 products are state-selectively probed, and the energy levels of the HOD coproduct are well-known.[25] By conservations of energy and momentum, the peak structure in the $P(\mu)$ distribution can easily be identified as the correlated vibration level of the HOD coproduct. As in part 1 of this series,[17] we denote the vibrational quantum number of HOD as ($v_{OD}v_{bend}v_{OH}$). Also shown in the figures are the contribution of each correlated vibration level (the dotted line) and the overall fitting (the solid line). Illustrated on the right

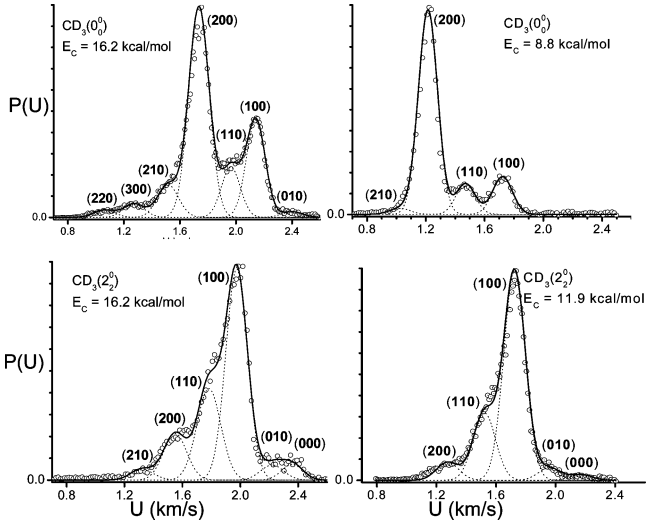

Figure 2. Four $P(\mu)$ distributions are exemplified. The upper panels are for the ground-state CD_3 product, and the lower two for the first overtone of umbrella-mode excited CD_3. The vibrational levels of the HOD coproduct are assigned as (υ_{OD} υ_{bend} υ_{OH}) on energetic grounds. The dotted line gives the contribution from each labeled level and the solid line represents the fit. Distinct patterns are readily observed for the two CD_3 states, whereas only minor differences are noted for the same CD_3 state at different collision energies.

are the two lower energy cases for $CD_3(\upsilon = 0)$ and ($\upsilon_2 = 2$), respectively. Comparing these $P(\mu)$ distributions with the results reported in part 1 of this series,[17] a general observation emerges: for a given $CD_3(\upsilon)$ state, the correlated HOD vibrational distribution, which is quite distinct for the tagged CD_3 state, is not particularly sensitive to initial collision energies—except that more minor levels are produced at higher E_c.

This general observation can be quantified by examining the correlated vibrational branching, as summarized in Figure 3. (To avoid congestion, the results in part 1 of this series[17] are excluded here.) As is seen, the spread of the vibrational distribution at higher collision energies is mainly among the pure stretching mode of excitations at the expense of the most prominent state. The extent of the bending- and combination-modes of excitations in each case is in general less sensitive to the variations in initial collision energy than pure stretch. Figure 4 elucidates such results for the two CD_3 product states in another way. Plotted here are the collisional energy dependencies of the ratio of (bend + combination)/(pure stretch) of the correlated HOD products. While the ratios for $CD_3(\upsilon_2 = 2)$ are high and display a mild dependence on the change in E_c, those for $CD_3(\upsilon = 0)$ exhibit a clear increase with the increase in E_c. The previously reported mode correlation that an umbrella-excited CD_3 product is preferentially accompanied by a HOD coproduct with higher probability in bend/combination mode of excitation[17] is, by and large, retained over a wide range of collisional energies.

(B) Correlated Energy Disposal. Figure 5 summarizes the collisional energy dependencies of the energy disposal into correlated HOD internal energy and product kinetic energy release. The tagged CD_3 product state is labeled on top of the column, and the lower panel shows the average energy disposals into the vibrational (V'), rotational (R') motions of HOD coproducts, and the average kinetic energy release (T') of the two products. Both V' and T' are derived directly from image analysis, whereas R' is deduced by the conservation of energy. The exothermicity of this reaction is 13.73 kcal/mol, and the reaction threshold is around 5 kcal/mol (vide infra). When CD_3 is produced in the vibrational ground state, the correlated

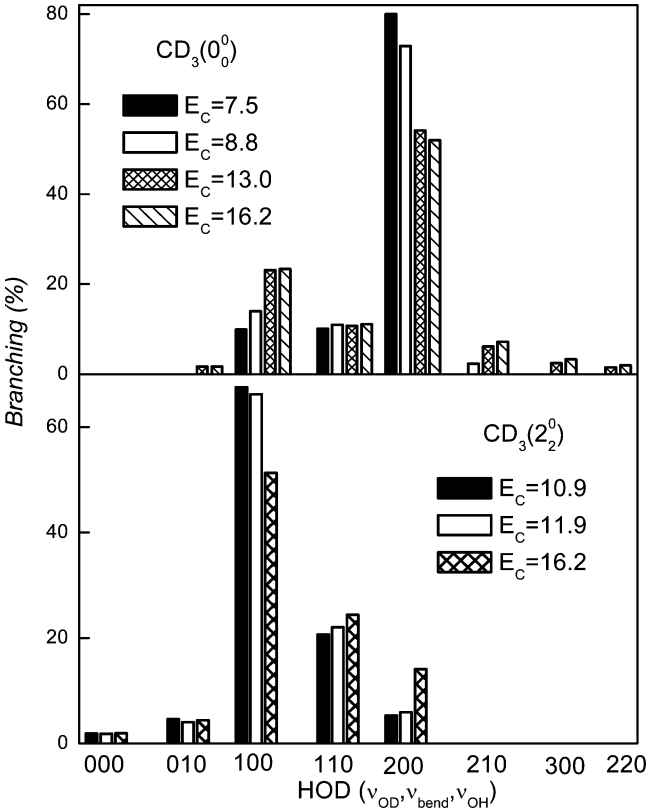

Figure 3. Summary of the vibrational branching of HOD correlated to the product states, $CD_3(\upsilon = 0)$ and $CD_3(\upsilon_2 = 2)$. For clarity, the results reported in part 1 of this series[17] are not depicted here.

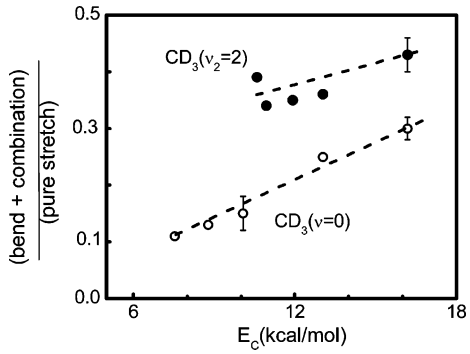

Figure 4. Collisional energy dependencies of the (bend + combination)/(pure stretch) ratio of the correlated HOD products for the two CD_3 product states. The error bars encompass the uncertainties from two independent measurements as well as in fitting the $P(\mu)$ distributions.

rotational energy of HOD coproducts hardly changes at all over the full collision energy range of this study. Similar behavior is seen for the average vibrational energy of HOD, except near threshold, and the coincidently formed HOD is always highly vibrational-excited. Because of near invariance of V' and R' with respects to E_c, the amounts of increase in total available energy at higher E_c almost all channel into T', yielding a linear dependence on E_c as shown. The finding of a $\Delta T \rightarrow \Delta T'$ propensity is reminiscent of one of Polanyi's rules, $\Delta T \rightarrow \Delta T' + \Delta R'$ that is based on atom + diatom reactions[27] and has a kinematic origin as discussed previously for both more exothermic reaction F + CD_4/CHD_3[28,29] and slightly endothermic reaction Cl + CH_4/CD_4.[30,31] In brief, the reaction essentially invokes a D atom transfer from CD_4 to the attacking OH; thus, a heavy + light-heavy system. If one further treats the CD_3 moiety as a structureless particle, one has then, in the spectator

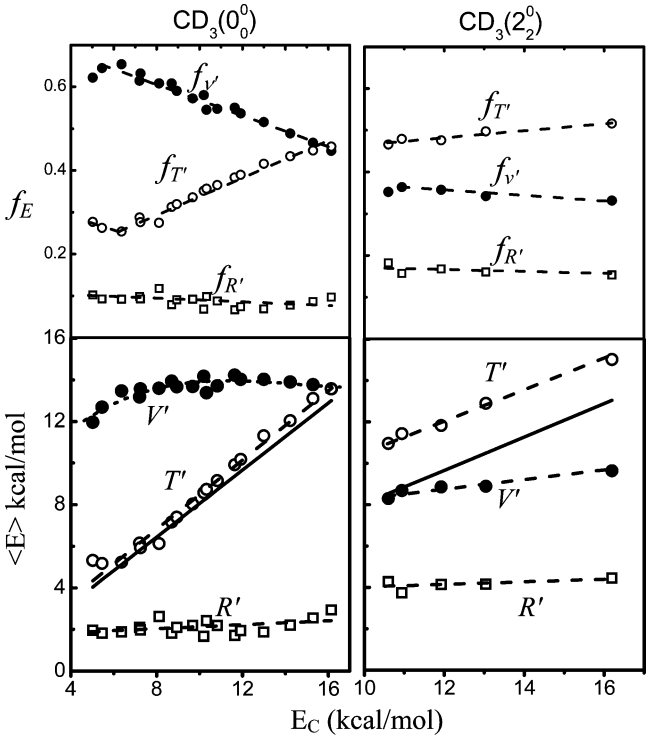

Figure 5. Summary of the correlated energy disposal for the two CD_3 product states. Shown in the lower panels is the absolute energy disposal. The dashed lines are to guide the eyes, and the solid lines are from a kinematic spectator model. The upper panels give the fractional energy disposals.

limit of a direct exothermic A + BC → AB + C reaction, $T' = E_c \cos^2 \beta$ with $\cos^2 \beta = m_A m_C/(m_A + m_B)(m_B + m_C)$.[32] The prediction of this simple spectator model is depicted in the figure as the solid line for comparison. Clearly, the key experimental observation can largely be accounted for by this kinematic consideration.

As to the umbrella-excited $CD_3(v_2 = 2)$, a quite different pattern in correlated energy disposal is seen. While the average rotational energies of the HOD coproducts remain roughly constant, they are about twice as large the $CD_3(v = 0)$ case. In addition, both V' and T' increase linearly, to different extents, with the increase in E_c. Compared to the $CD_3(v = 0)$ case over the same E_c range, the propensity switches from $V' > T'$ for $CD_3(v = 0)$ to $T' > V'$ for $CD_3(v_2 = 2)$. Similarly, assuming the methyl moiety can be treated as a spectator—it now remains as $CD_3(v_2 = 2)$ with the change in E_c, the solid line gives the result of the kinematic model. It is interesting to note that the simple model predicts the same dependency or slope as the experimental observation, but offsets *downward* by a constant value of ~2.6 kcal/mol that intriguingly (or fortuitously) is about the same as the vibrational energy of 2.76 kcal/mol for $CD_3(v_2 = 2)$. Intuitively, one might have expected an opposite trend of observing less T' because part of the available energy has been deposited into $CD_3(v_2 = 2)$. Instead, there is an excess T' for the formation of $CD_3(v_2 = 2)$. In other words, when CD_3 is produced with two-quantum excitation of umbrella mode, the coincidently formed HOD possesses a substantially relaxed vibrational content, and the loss in vibrational energy is shared by R' and T' in a roughly equal manner.

Because the available energy for disposal at the same E_c is less for the $CD_3(v_2 = 2)$ + HOD pair than $CD_3(v = 0)$ + HOD, the contrast between the two channels can be better appreciated by the fractional energy disposal f_E as displayed in the upper two panels. For both the ground and umbrella-excited CD_3, the

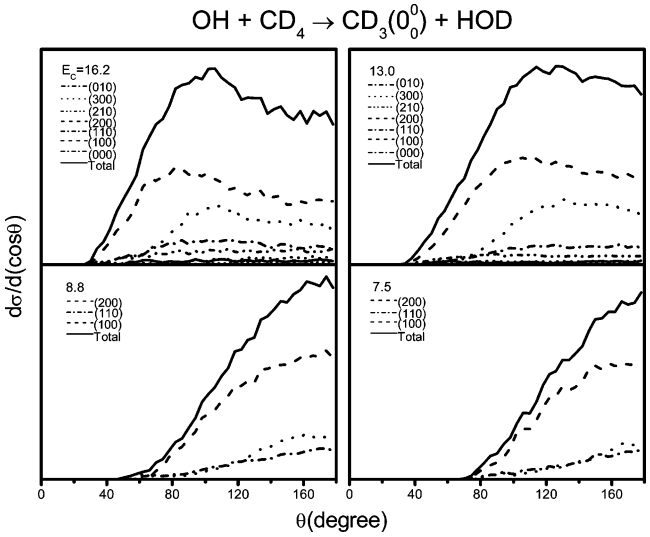

Figure 6. State-correlated angular distributions for the ground-state reaction at four different collision energies.

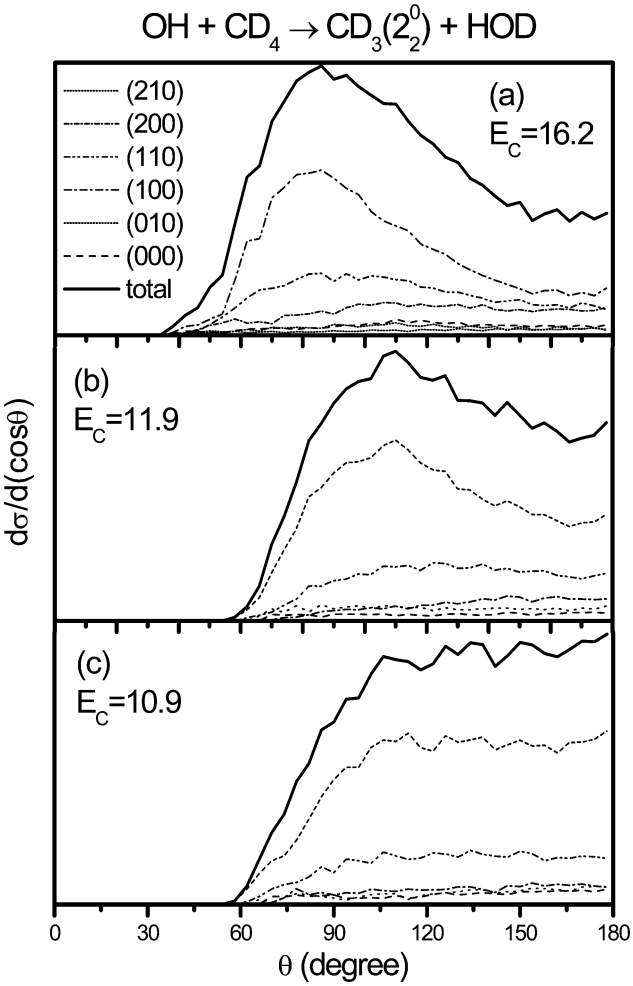

Figure 7. As in Figure 6, but for probing the $CD_3(v_2 = 2)$ product state at three collisional energies.

fractional excitation of the correlated HOD rotors remains roughly constant as E_c increases. And the latter case yields a value of about two times as large the former. As to the fractional energy disposal into the correlated HOD vibrators, both exhibit declined trends with the increases in E_c. This trend is more pronounced for the $CD_3(v = 0)$ case − $f_{V'}$ descends from about 65% near threshold to ~ 45% at E_c = 16 kcal/mol, whereas

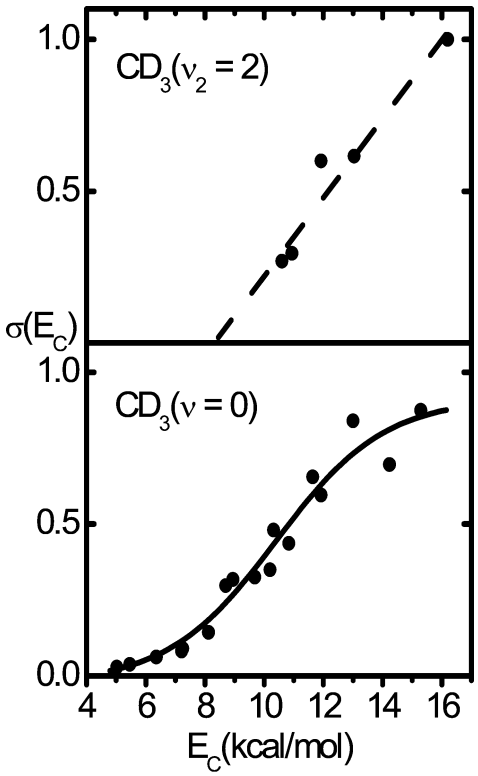

Figure 8. Total reactive excitation functions for the two CD_3 product vibrational states as indicated. The experimental data for $CD_3(v = 0)$ consist of three independent measurements/analysis at different days. The scatters of the data points represent the errors, both statistical and systematic, of our determination. Two excitation functions are not normalized to each other. A reaction threshold of ~5 kcal/mol can be deduced.

the $f_{V'}$(HOD) for $CD_3(v_2 = 2)$ is significantly smaller and shows much less variation − only a few percentages. For the product kinetic energy release, the $f_{T'}$ for the $CD_3(v_2 = 2)$ + HOD pair accounts for about 50% of the available energy and displays a mild ascendancy. In the case of $CD_3(v = 0)$, on the other hand, the $f_{T'}$ shows a dramatic increase from about 25% near threshold to 45% at 16 kcal/mol.

In part 1 of this series, (ref 17), we interpreted the observed mode correlation of product pairs for $CD_3(v_2 = 2)$ + HOD(v') and $CD_3(v = 0)$ + HOD(v') as the result of different reaction pathways driven by dynamics in the transition state region. In that view, the formation of $CD_3(v_2 = 2)$ preferentially involves larger impact-parameter collisions with wider cone-of-acceptance, which mediated the colliding pair to attain more readily the transitory exit channel van der Waals complex allowing more intracomplex energy redistribution as the products are formed. The different behaviors in correlated energy disposals for $CD_3(v = 0)$ and $CD_3(v_2 = 2)$ shown in Figures 4 and 5 are consistent with the proposed picture, and further indicate its validity over a range of initial collision energies.

(C) Pair-Correlated Angular Distributions. The state-correlated angular distributions at different collision energies are shown in Figures 6 and 7 for $CD_3(v = 0)$ and $(v_2 = 2)$, respectively. The total angular distribution for $CD_3(v = 0)$, Figure 6, shifts systematically from backward peaking at E_c = 7.5 kcal/mol to sideways dominance at 16.2 kcal/mol. This trend corroborates very well with that in the previous communication at E_c = 10.0 kcal/mol.[17] In terms of pair-correlated angular distributions (CDCS), only small variations among the individual CDCS are noted at the two lower E_c's. Again, this finding is in line with the previous observation at 10.0 kcal/mol.[17] The CDCS shown for the two higher E_c's, however, display noticeable differences. While the distributions of the minor channels are generally rather flat within the backward hemisphere, the two dominant channels exhibit peaks away from the backward direction, resulting in the gradual shift of the total angular distribution toward sideways as noted above. Moreover, this shift-toward-sideways is apparently more pronounced for the most populated (200) state than the (100) state.

As to the $CD_3(v_2 = 2)$ state, the same qualitative trends with the increase in E_c are noted in Figure 7. Again, the general patterns are in excellent agreement with the earlier results at E_c = 10.6 and 13.0 kcal/mol.[17] Compared the angular distributions for the two CD_3 states, $(v = 0)$ and $(v_2 = 2)$, both are confined in the backward/sideways directions with a sharp cutoff against forward scattering, which suggests collisions of low reaction probability with severe steric hindrance. At the same collision energies, the umbrella-excited CD_3 products generally display a broader angular distribution, which also exhibit significantly more sideway peaking with the increase in E_c than the ground-state ones. This difference, as conjectured previously,[17] may reflect a wider cone-of-acceptance for the formation of $CD_3(v_2 = 2)$.

(D) Excitation Functions and $\sigma(\theta)$—θ—E_c Plots. The state-specific excitation functions for the vibrational ground and the

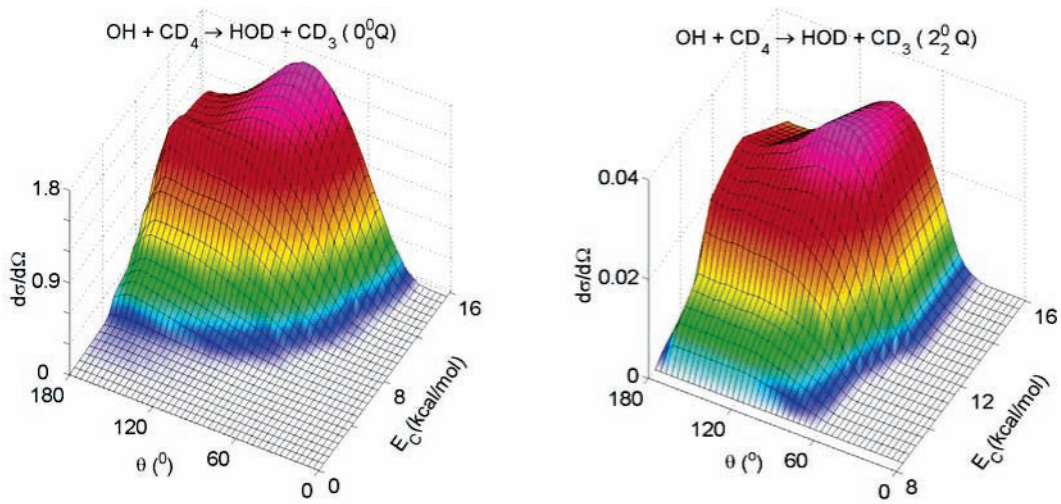

Figure 9. Three-dimensional representation of the dependencies of the product angular distributions on both scattering angles and collisional energies. Note the different ranges of E_c in the two plots.

umbrella-excited CD_3 products are presented in Figure 8. The experimental procedure to acquire such information is the same as that detailed previously.[33] Because of the uncertainty in relative sensitivity of the two REMPI probes, the excitation functions of $CD_3(0_0°)$ and $CD_3(2_2°)$ are not normalized to each other. For the ground-state $CD_3(v = 0)$ product, the reactive cross section increases very slowly near the threshold of ~5 kcal/mol, and rises more rapidly from $E_c \sim 8$ kcal/mol, and finally tends to level-off at E_c ~14 kcal/mol. The observed reaction threshold, ≤5 kcal/mol, compares favorably with the thermal activation energy of 4.2 kcal/mal for $OH + CD_4$.[34] As to the $CD_3(v_2 = 2)$ product, owing to much weaker signals, only five measurements at different E_c were performed. Thus, just an approximate energy dependency of its cross section can be derived, as shown in Figure 8. For clarity, the individual state-correlated excitation function is not depicted here because of the similar shape.

The combination of excitation function with angular distribution has proven particularly insightful for a number of reactions[30,31,35] by offering a global view of reaction dynamics through the $\sigma(\theta;E_c)-\theta-E_c$ plot. Such plots for the present cases are depicted in Figure 9. The characteristic appearance, i.e., a broad swath in the backward hemisphere, provides an unequivocal evidence for a typical direct rebound reaction mechanism, for both product pairs, over the energy range of this study. It is instructive to compare Figure 9 with those from another direct reactions of $Cl + CD_4/CH_4$ (Figure 7 of ref 31), especially for the intriguing difference in the general appearances of the swaths. In this regard, we will also call attention to the distinct pattern of the $Cl + CH_4 \rightarrow CH_3(v = 0) + HCl\ (v' = 1)$ reaction, for which a dynamical resonance mechanism was proposed.[30]

IV. Conclusions

An extensive study of the reaction dynamics of $OH + CD_4 \rightarrow CD_3 + HOD$ over a wide range of collision energies, 5−16 kcal/mol, was reported here. The intriguing mode correlation between the product pairs, discovered previously in part 1 of this series,[17] was found to persist over the full energy range of this study. That correlation can be summarized as the following. The HOD products concomitantly formed with $CD_3(v = 0)$ are highly vibrational-inverted with predominant excitation in the pure stretching mode of the newly born OD bond. When CD_3 is produced with umbrella mode of excitation, the correlated vibrational contents of HOD coproducts become markedly less, but the populations in the bending and combination modes increase significantly. As in part 1 of this series,[17] we interpreted the observed mode correlation as the result of a bifurcation of the subtle reaction pathways driven by dynamics in passing through the transition state region. The collisional energy dependencies of several correlated attributes, including reaction cross section, vibrational state distribution, energy disposal, and angular distribution are elucidated in details. In the following paper, the isotope effects in this reaction will be scrutinized. Together, these studies might constitute one of the most comprehensive experimental characterizations of a polyatomic reaction system.

Acknowledgment. This work was supported by the National Science of Council of Taiwan under NSC 93-2113-M-001-041 and NSC 94-2915-I-001-011. B.Z. gratefully acknowledges Academia Sinica for a postdoctoral fellowship.

References and Notes

(1) Glassman, I. *Combustion*, 3rd ed.; Academic Press: San Diego, CA, 1996.
(2) Campbell, I. M. *Energy and the Atmosphere*; John Wiley & Sons Ltd.: London, 1977.
(3) Wayne, R. P. *Chemistry of Atmospheres*, 2nd ed.; Oxford University Press: Oxford, U.K., 1991.
(4) Vaghjiani, G. L.; Ravishankara, A. R. *Nature (London)* **1991**, *350*, 406.
(5) Ravishankara, A. R. *Annu. Rev. Phys. Chem.* **1988**, *39*, 367.
(6) Baulch, D. L.; Cobos, C. J.; Cox, R. A.; Esser, C.; Frank, P.; Just, Th.; Kerr, J. A.; Pilling, M. J.; Troe, J.; Walker, R. W.; Warrnatz, J. *J. Phys. Chem. Ref. Data* **1992**, *21*, 411.
(7) Srinivasan, N. K.; Su, M.-C.; Sutherland, J. W.; Michael, J. V. *J. Phys. Chem. A* **2005**, *109*, 1857 and references therein.
(8) Bravo-Perez, G.; Alvarez-Idaboy, J. R.; Jimenez, A. G.; Cruz-Torres, A. *Chem. Phys.* **2005**, *310*, 213.
(9) Espinosa-Garcia, J.; Corchado, J. C. *J. Chem. Phys.* **2000**, *112*, 5731.
(10) Masgrau, L.; Gonzalez-Lafont, A.; Lluch, J. M. *J. Chem. Phys.* **2001**, *114*, 2154; *Theor. Chem. Acc.* **2002**, *108*, 38.
(11) Jursic, B. S. *J. Chem. Soc., Faraday Trans.* **1996**, *92*, 3467.
(12) Corchado, J. C.; Coitino, E. L.; Chuang, Y.-Y.; Fast, P. L.; Truhlar, D. G. *J. Phys. Chem. A* **1998**, *102*, 2424.
(13) Chuang, Y.-Y.; Coitino, E. L.; Truhlar, D. G. *J. Phys. Chem. A* **2000**, *104*, 446.
(14) Nyman, G.; Clary, D. C. *J. Chem. Phys.* **1994**, *101*, 5756.
(15) Nyman, G.; Clary, D. C.; Levine, R. D. *Chem. Phys.* **1995**, *191*, 223.
(16) Yu, H.-G. *J. Chem. Phys.* **2001**, *114*, 2967.
(17) Zhang, B.; Shiu, W.; Lin, J. J.; Liu, K. *J. Chem. Phys.* **2005**, *122*, 131102. (Part 1 of this series).
(18) Strazisar, B. R.; Lin, C.; Davis, H. F. *Science* **2000**, *290*, 958.
(19) Zhang, D. H.; Collins, M. A.; Lee, S.-Y. *Science* **2000**, *290*, 961.
(20) Castillo, J. F. *Chem. Phys. Chem.* **2002**, *3*, 320.
(21) Zhou, J.; Lin, J. J.; Liu, K. *J. Chem. Phys.* **2003**, *119*, 8289.
(22) Lin, J. J.; Zhou, J.; Shiu, W.; Liu, K. *Rev. Sci. Instrum.* **2003**, *74*, 2495.
(23) Zhou, J.; Lin, J. J.; Shiu, W.; Pu, S.-C.; Liu, K. *J. Chem. Phys.* **2003**, *119*, 2538.
(24) Even, U.; Jortner, J.; Noy, D.; Lavie, N.; Cossart-Magos, C. *J. Chem. Phys.* **2000**, *112*, 8068.
(25) Smith, D. F., Jr.; Overend, J. *Spectrochim. Acta* **1972**, *28A*, 471.
(26) Lin, J. J.; Zhou, J.; Shiu, W.; Liu, K. *Science* **2003**, *300*, 966.
(27) Polanyi, J. C. *Science* **1987**, *236*, 860; *Acc. Chem. Res.* **1972**, *5*, 161.
(28) Zhou, J.; Lin, J. J.; Shiu, W.; Liu, K. *J. Chem. Phys.* **2003**, *119*, 4997.
(29) Zhou, J.; Lin, J. J.; Liu K. *J. Chem. Phys.* **2004**, *121*, 813.
(30) Zhang, B.; Liu, K. *J. Chem. Phys.* **2005**, *122*, 101102.
(31) Zhou, J.; Zhang, B.; Lin, J. J.; Liu, K. *Mol. Phys.* **2005**, *103*, 1757.
(32) Valentini, J. J. *J. Phys. Chem. A* **2002**, *106*, 5745.
(33) Shiu, W.; Lin, J. J.; Liu, K.; Wu, M.; Parker, D. H. *J. Chem. Phys.* **2004**, *120*, 117.
(34) Gierczak, T.; Talukdar, R. K.; Herndon, S. C.; Vaghjiani, G. L.; Ravishankara, A. R. *J. Phys. Chem.* **1997**, *101*, 3125.
(35) Skodje, R. T.; Skouteris, D.; Manolopoulos, D. E.; Lee, S.-H.; Dong, F.; Liu, K. *Phys. Rev. Lett.* **2000**, *85*, 1206.